Cross Sections for Electron Collisions with NF$_3$

Mi-Young Song, Jung-Sik Yoon, Hyuck Cho, Grzegorz P. Karwasz, Viatcheslav Kokoouline, Yoshiharu Nakamura, James R. Hamilton, and Jonathan Tennyson

---

Articles you may be interested in

Cross Sections for Electron Collisions with Ammonia
Journal of Physical and Chemical Reference Data **46**, 043103 (2017); 10.1063/1.5001918

Cross Sections for Electron Collisions with Acetylene
Journal of Physical and Chemical Reference Data **46**, 013106 (2017); 10.1063/1.4976569

Insights to scaling remote plasma sources sustained in NF$_3$ mixtures
Journal of Vacuum Science & Technology A: Vacuum, Surfaces, and Films **35**, 031302 (2017); 10.1116/1.4978551

Overview of atomic layer etching in the semiconductor industry
Journal of Vacuum Science & Technology A: Vacuum, Surfaces, and Films **33**, 020802 (2015); 10.1116/1.4913379

Evolution of electron temperature in inductively coupled plasma
Applied Physics Letters **110**, 014106 (2017); 10.1063/1.4971980

On the Melting Curve of Sulfur Hexafluoride
Journal of Physical and Chemical Reference Data **46**, 043102 (2017); 10.1063/1.5005537

Cross Sections for Electron Collisions with NF_3

Mi-Young Song[a)] and Jung-Sik Yoon

Plasma Technology Research Center, National Fusion Research Institute, 814-2, Osikdo-dong, Gunsan, Jeollabuk-do 573-540, South Korea

Hyuck Cho

Department of Physics, Chungnam National University, Daejeon 305-764, South Korea

Grzegorz P. Karwasz

Faculty of Physics, Astronomy and Applied Informatics, University Nicolaus Copernicus, Grudziadzka 5, Toruń 87-100, Poland

Viatcheslav Kokoouline

Department of Physics, University of Central Florida, Orlando, Florida 32816, USA

Yoshiharu Nakamura

6-1-5-201 Miyazaki, Miyamae, Kawasaki 216-0033, Japan

James R. Hamilton, and Jonathan Tennyson

Department of Physics and Astronomy, University College London, Gower Street, London WC1E 6BT, United Kingdom

Cross section data are compiled from the literature for electron collisions with nitrogen trifluoride (NF_3) molecules. Cross sections are collected and reviewed for total scattering, elastic scattering, momentum transfer, excitations of rotational and vibrational states, dissociation, ionization, and dissociative attachment. For each of these processes, the recommended values of the cross sections are presented. The literature has been surveyed until end of 2016. © *2017 AIP Publishing LLC for the National Institute of Standards and Technology.* https://doi.org/10.1063/1.5000687

CONTENTS

List of Tables

[a)]Author to whom correspondence should be addressed; electronic mail: mysong@nfri.re.kr.

List of Figures

1. Introduction

Nitrogen trifluoride or trifluoramine (NF_3) gas is widely used in plasma processing technology. NF_3 is used in a number of plasma processes where it is often used as a source of F atoms due to ease of production of these atoms via dissociative electron attachment (DEA) and electron-impact dissociation both from NF_3 itself and from NF_2 and NF fragment species. The exothermicity from these dissociative processes also provides an important gas heating mechanism. Use of NF_3 in plasma etching, particularly in mixtures with O_2, see Ref. 1, provides a source of F^- ions due to an enhanced DEA process at low (about 1 eV) energies. NF_3 is widely used for semiconductor fabrication processes which include direct etching,[2,3] reactor cleaning,[4] and remote plasma sources,[5] where use of pure NF_3 typically limits the reactants reaching the processing chamber only to F_x and NF_x species. NF_3 is also used in the production of thin films[6,7] and solar cells;[8,9] it provides the initial gas for the HF chemical laser.[10–12] NF_3 is actually a greenhouse gas with a very high global warming potential which has led to concern on how it is used in the various technologies discussed above.[13] In spite of its importance, experimental studies of electron scattering on NF_3 are rather sparse: for total[14] and elastic[15] cross section measurements coming from single laboratories, more measurements exist for ionization[16–18] and DEA.[19–21] In the absence of experiments, several calculations[22–25] have been performed. Some reference cross sections based both on experiments and calculations were reported by Lisovskiy *et al.*[26] in modeling electron transport coefficients and by Huang *et al.*[1] for modeling remote plasma sources in NF_3 mixtures. Here we perform a detailed analysis of available data for electron scattering on NF_3, to yield recommended total, elastic, momentum transfer, ionization, dissociation into neutrals, and vibrational, rotational, and electronic excitation cross sections. In the ground electronic state $^1A'$, the molecule has a shape of a pyramid of the C_{3v} group with fluorine atoms forming an equilateral triangle. Due to its symmetry, the dipole moment of the molecule is aligned along the C_3 symmetry axis. Geometry, electric dipole moment, and rotational constants are specified in Table 1.

2. Total Scattering Cross Section

Practically, absolute data by Szmytkowski *et al.*[14] at 0.5–370 eV collision energy is the only measurement of total cross section (TCS) in NF_3. The beam attenuation from deBeer Lambert's method was used, with a 3 cm-long scattering cell and 2×10^{-3} sr mean angular resolution. Systematic errors declared (gas outflow from the scattering cell, determination of the scattering length, current non-linearity, and pressure and temperature measurements) are within 5%,

TABLE 1. Properties of NF_3 at the equilibrium position of the ground electric state. A, B, and C are rotational constants; α_0 is the spherical dipole polarizability

Property	Value
F–N bond length[27]	1.365 Å
FNF angle[27]	102.4°
Dipole moment[27]	0.235 D
$A = B$[28]	10.681 081 9(15) GHz
C[28]	5.8440 GHz
α_0[29]	3.62×10^{-30} m³

out of which the declared angular resolution error is 0.2% at low energies, rising to 1% at 100 eV and 2%–3% in the high energy limit. The statistical spread (one standard deviation of their weighted mean values) is 1.5% below 1 eV and below 1% at intermediate energies. TCSs[14] are compared to experimental elastic cross sections,[15] ionization,[18] and vibrational excitation (calculated in the Born approximation) in Fig. 1.

Calculations of integral elastic cross sections[24,25] predict a resonance structure which is much narrower (and higher) than the resonance seen in the TCS;[14] see Fig. 1. This may be due to the neglect of nuclear motion in the calculations. Similar discrepancies between theory and experiments are observable for molecular targets, such as CO_2 and N_2O: in these molecules, the vibrational excitation constitutes a significant part (about 1/3) of the TCS.[31] Calculations for N_2O,[32] similar to those for NF_3, also give resonant maxima higher than those of the experiment. Note also that NF_3 is a polar molecule, so the interaction with the incoming electron is more attractive in comparison to targets like CH_4, and this shifts maxima to lower energies. Two recent calculations[24,25] indicate that the TCS should rise in the limit of zero energy due to the polar character of the molecule. Unfortunately, this was not observed in the experiment,[14] probably because the measurements were stopped at energies higher than the range of such a rise. The rather poor angular resolution of the apparatus of Szmytkowski *et al.* makes their measurement vulnerable to the angular resolution error at high energies. To verify this, in Fig. 2, we show a Bethe–Born plot of TCSs, as done in our previous review on CH_4,[33]

$$\sigma(E) = A/E + B \log(E)/E, \qquad (1)$$

where energy is expressed in Rydbergs, Ry $= 13.6$ eV, and the cross sections are expressed in atomic units $a_0^2 = 0.28 \times 10^{-16} cm^2$. Parameters of the fit based on experimental points[14] between 100 and 220 eV are $A = -110 \pm 10$ and $B = 610 \pm 20$. Contrary to expectations, the plot in Fig. 2 suggests that TCSs given by Szmytkowski *et al.*[14] are
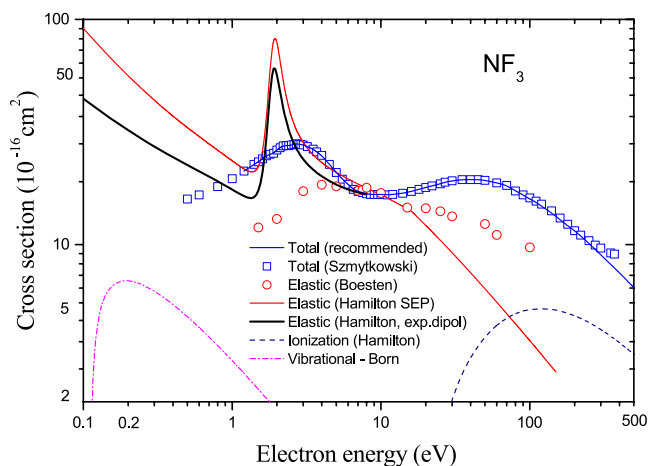
FIG. 1. TCSs by Szmytkowski *et al.*[14] compared to experimental integral elastic cross sections of Boesten *et al.*,[15] integral vibrational excitation (Born approximation for the ν_3 IR active mode), and total ionization (theory by Rahman *et al.*[18]).
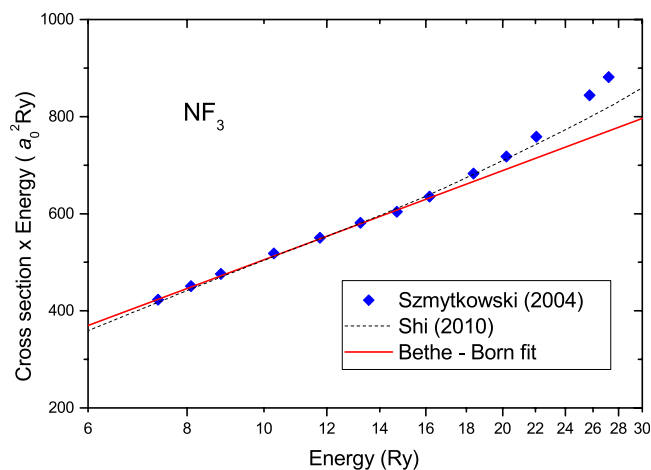
FIG. 2. Bethe–Born plot of TCSs by Szmytkowski *et al.*[14] in their high energy limit. TCSs from the modified additivity rule of Shi *et al.*[30] are also shown for comparison (data read from their Fig. 1).

overestimates in their high energy limit. We note however that Bethe–Born analysis is not fully justified at energies of few hundreds of eV; see discussion in Refs. 34 and 35. Therefore, in Fig. 2, we also plot TCSs obtained by the additivity rule:[30] these data coincide with the present Bethe–Born fit up to 200 eV and then deviate slightly upwards. Unfortunately, no information on uncertainties was given by Shi *et al.*[30] Table 2 gives our recommended TCSs which are based on the experiment in Ref. 14 at energies 1–90 eV and on the Bethe–Born fit at higher energies.

TABLE 2. Recommended TCSs in 10^{-16} cm² units. In the region 1–100 eV, recommended values are adopted from the experiment by Szmytkowski *et al.*[14] Values at 100–500 eV are obtained from parameters of the Bethe–Born plot, Fig. 2. The overall uncertainty of TCS is ±10% at 1–100 eV and 15% above 100 eV. Additionally from the ±10% uncertainty, TCSs below 1 eV[14] may be underestimated due to an angular resolution error, by the amount rising with lowering energy. The energy determination is ±0.1 eV

Electron energy	TCS	Electron energy	TCS	Electron energy	TCS
0.5	15.9	3.7	25.8	35	19.4
0.6	16.6	4.0	24.9	40	19.4
0.8	18.1	4.5	22.7	45	19.4
1.0	19.6	5.0	20.9	50	19.3
1.2	21.2	5.5	19.5	60	18.8
1.4	22.7	6.0	18.5	70	18.3
1.5	23.3	6.5	17.6	80	17.3
1.6	24.0	7.0	17.2	90	16.6
1.7	24.8	7.5	17.0	100	15.9
1.8	25.2	8.0	16.8	110	15.4
1.9	25.4	8.5	16.7	120	14.8
2.0	26.3	9.0	16.7	140	13.8
2.1	26.9	9.5	16.7	160	12.9
2.2	27.4	10	16.7	180	12.1
2.3	27.5	11	16.6	200	11.5
2.4	27.5	12	16.7	220	10.9
2.5	27.7	14	16.9	250	10.1
2.6	27.8	16	17.2	275	9.51
2.7	28.0	18	17.6	300	9.00
2.8	27.9	20	17.9	350	8.16
2.9	27.8	22	18.2	400	7.48
3.0	27.7	25	18.6	450	6.91
3.2	27.2	27	18.9	500	6.43
3.5	26.5	30	19.2		

TABLE 3. Recommended elastic electron scattering cross sections from NF_3. DCSs are in the units of 10^{-16} cm^2 sr^{-1}. Recommended elastic ICSs are also given at the bottom in the units of 10^{-16}cm^2 (Ref. 15). The uncertainties of DCSs are 15% and of ICSs are 30%–50%

Angle (deg)	1.5 eV DCS	2 eV DCS	3 eV DCS	4 eV DCS	5 eV DCS	7 eV DCS	7.5 eV DCS	8 eV DCS	10 eV DCS	15 eV DCS	20 eV DCS	25 eV DCS	30 eV DCS	50 eV DCS	60 eV DCS	100 eV DCS
15	...	...	...	...	...	...	...	...	3.323	4.641	6.890	9.051	10.710	12.330	11.200	9.000
20	0.933	1.430	2.199	2.960	2.729	2.671	2.896	2.908	3.168	3.946	5.006	6.490	6.946	6.715	5.955	3.201
30	0.667	1.216	2.436	2.949	2.807	2.932	3.036	3.132	3.037	3.077	2.777	2.863	2.657	1.838	1.243	0.851
40	0.656	1.078	2.331	2.822	2.577	2.868	2.731	2.699	2.680	2.107	1.680	1.358	1.004	0.666	0.671	0.623
50	0.729	1.197	2.052	2.511	2.119	2.123	2.224	2.115	1.934	1.271	0.934	0.742	0.616	0.621	0.537	0.340
60	0.787	1.152	1.768	1.818	1.552	1.655	1.517	1.460	1.390	0.826	0.750	0.688	0.639	0.601	0.328	0.195
70	0.962	1.074	1.329	1.297	1.261	1.137	1.108	1.209	0.954	0.715	0.799	0.747	0.671	0.340	0.232	0.156
80	0.981	1.100	1.114	1.099	0.947	0.808	0.851	0.868	0.737	0.725	0.798	0.665	0.509	0.196	0.155	0.116
90	1.097	1.011	0.920	0.794	0.714	0.727	0.719	0.766	0.702	0.786	0.715	0.510	0.320	0.116	0.109	0.067
100	1.053	0.884	0.685	0.640	0.641	0.663	0.704	0.702	0.694	0.738	0.569	0.322	0.191	0.093	0.093	0.073
110	0.998	0.843	0.598	0.542	0.622	0.666	0.704	0.707	0.673	0.610	0.462	0.295	0.200	0.146	0.152	0.108
120	0.992	0.778	0.584	0.539	0.637	0.652	0.661	0.639	0.626	0.555	0.561	0.440	0.376	0.314	0.265	0.169
130	0.920	0.723	0.576	0.604	0.765	0.655	0.645	0.623	0.605	0.598	0.746	0.725	0.623	0.483	0.378	0.273
ICS	11.90	12.98	17.24	18.41	18.11	17.35	17.47	17.89	16.91	14.60	14.48	14.05	13.33	12.32	11.03	9.72
L%	4	5	7	7	8	7	8	13	6	9	13	18	24	35	41	47
R%	15	18	19	20	21	20	20	15	20	14	14	17	15	62	13	17

3. Elastic Scattering Cross Section

Available data for elastic electron scattering from NF_3 are very sparse. The first theoretical study on low-energy electron collision processes in NF_3 was reported by Rescigno[22] which included Kohn variation calculations of elastic differential cross sections (DCSs) and integral cross sections (ICSs) for electrons with energies in the range 0–10 eV. The only comprehensive experimental study, which reported elastic DCSs, ICSs, and momentum transfer cross sections (MTCSs) for energies between 1.5 and 100 eV and for angles between 15° (20° for energies below 8 eV) and 130°, was published by Boesten *et al.*[15] Subsequently, a Schwinger multichannel

theoretical approach[23] reported corresponding cross sections for electron energies in the range 0–60 eV. Complete numerical values of Boesten *et al.*[15] and four representative figures for DCSs are presented in Table 3 and Fig. 3. Their ICSs are also given in Table 3 and Fig. 4. Theoretical ICSs of Joucoski and Bettega[23] and the TCSs of Szmytkowski *et al.*[14] are plotted in Fig. 4 for comparison. Generally good agreement is found between the results from the calculation by Joucoski and Bettega and the experiment by Boesten *et al.*, except for a few points between 5 eV and 10 eV, where the theory exceeds the TCSs of Szmytkowski *et al.* The permanent dipole moments of NF_3 is 0.0944 a.u., which is small compared to other polar molecules such as NH_3 (0.578 a.u.)
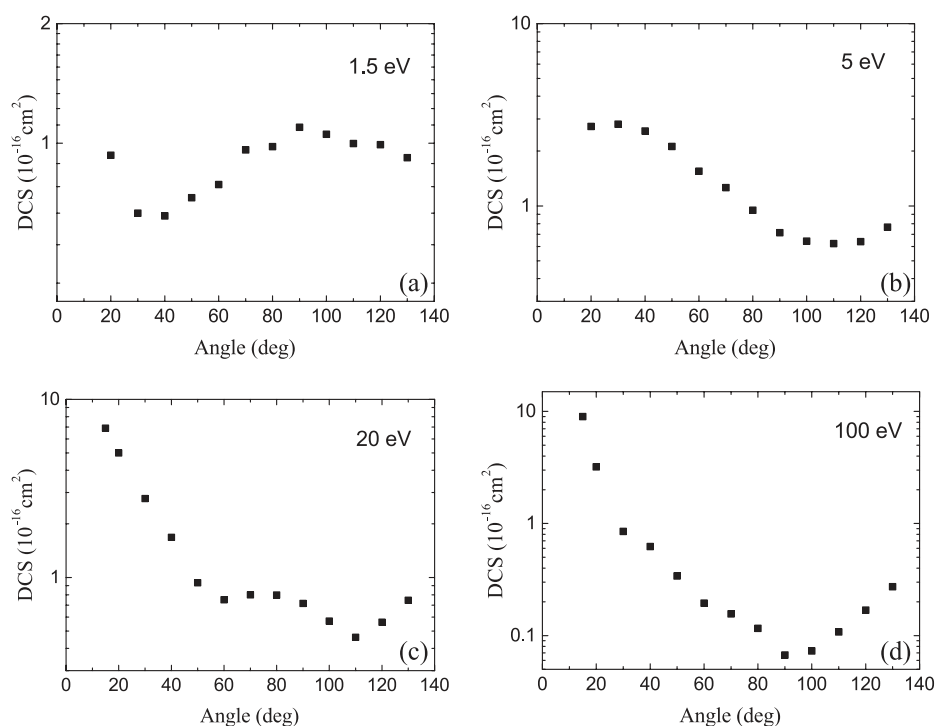

FIG. 3. Recommended elastic differential cross sections for four representative energies.[15]
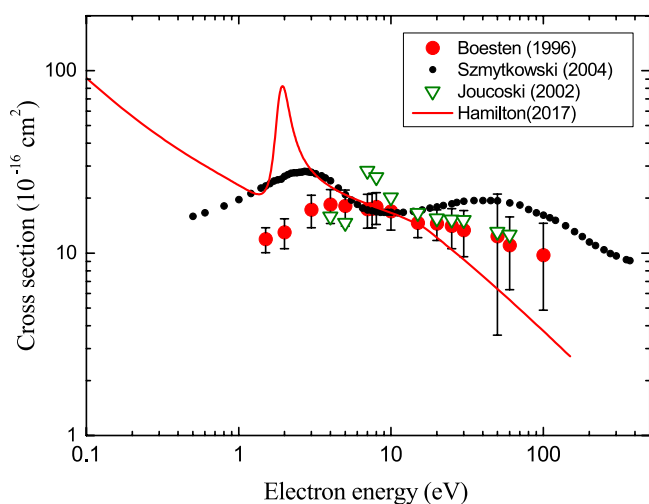
FIG. 4. Recommended elastic ICSs with the selected sets of data from the publications.[14,15,23,25]

FIG. 5. The MTCS for elastic collisions obtained in different studies. The recommended data are shown by the thick green line. The data are the theoretical results by Hamilton *et al.*[25] below 0.65 eV and the experimental results by Boesten *et al.*[15] above 1.5 eV.

and H_2O (0.728 a.u.). Therefore, dipole interaction between the electron and NF_3 would not be important in this collision system.[15] And, dipole-enhanced forward scattering is restricted to small angles, usually below 10°–20°, and Boesten *et al.* claimed that this was confirmed in the calculations of Rescigno[22] whose DCSs at 20° reflect their own data. In the energy and angular ranges of the experiments by Boesten *et al.*, there is no evidence that their results are unreasonably underestimated even though there could still be a few possibilities of slight over- or under-estimation which may not be included in their uncertainty estimation. So our recommended data are consequently taken from the measurements of Boesten *et al.* Similarly, we recommend their ICSs. Boesten *et al.* estimated the uncertainties of DCSs as 15% and of ICSs as 30%–50%. They estimated the contributions of the low and high angle extrapolations separately, and we present these in their original forms at the bottom of Table 3. The contributions of the low and high angle extrapolations are indicated as L% and R%, respectively. Very recently, Hamilton *et al.* published calculated ICSs,[25] and they are presented in Fig. 4 for comparison.

4. MTCS

The MTCS for electron–NF_3 collisions was determined in the same studies, mentioned above,[15,22,23,25] where the elastic cross sections were measured or computed. The experimental data by Boesten *et al.*[15] are not complete, especially, at energies below 1 eV. Out of the three theoretical studies,[22,23,25] the most recent one by Hamilton *et al.*[25] appears to be the most accurate one due to a more accurate method (complete active space-configuration interaction) and a larger basis set employed. However, the position of the resonance near 1 eV in this study is shifted towards lower energies compared to the experimental data. The width of the resonance in all theoretical studies is significantly narrower than that in the experiment. Therefore, at energies above 1 eV, where experimental data exist, we recommend the experimental data, namely, the one by Boesten *et al.*[15] and at energies below 1 eV, the theoretical results by
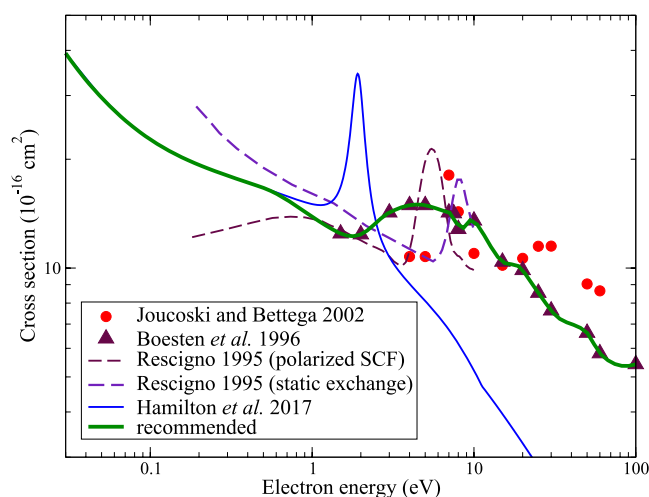
Hamilton *et al.*[25] The available theoretical and experimental data, as well as the recommended set, are shown in Fig. 5. The values of the recommended data are given in Table 4. Lisovskiy *et al.*[26] measured the drift velocity of electrons in NF_3 in a limited range of high reduced electric field E/p and compared their measurements with the results of the BOLSIG+ calculations using the MTCSs of Boesten *et al.*[15] and Joucoski and Bettega.[23] Agreement was satisfactory, especially with the calculation using the latter MTCS.

5. Rotational Excitation Cross Section

Due to its C_{3v} symmetry at equilibrium geometry, NF_3 is a symmetric top in the rigid-rotor approximation. It is an oblate rotor with rotational constants given in Table 1. As for other symmetric top molecules, the rotational levels of NF_3 are characterized by two quantum numbers, the rotational angular momentum j, and its projection k on the molecular symmetry axis. The fluorine atom has only one stable isotope, ^{19}F with nuclear spin $i = 1/2$. Therefore, the total nuclear spin of three fluorine atoms could be $I = 1/2$ (para-NF_3) or $3/2$ (ortho-NF_3). In the following discussion, we neglect the hyperfine interaction and mixing between singlet and triplet nuclear-spin states of NF_3. The total wave function, including the nuclear-spin part, of NF_3 should be of the A_2 irreducible representation of the C_{3v} group because ^{19}F is a fermion. It means that for ortho-NF_3, the space part (rovibronic) of the wave function should also be of the A_2 irreducible representation because the nuclear-spin part is totally symmetric, A_1. For para-NF_3, the space part of the wave function should be of the E irreducible representation. In both the cases, it leads to the conclusion that the lowest allowed rotational level in the ground *vibronic* state has $j = 1$. The $j = 0$ rotational level is forbidden for the ground *vibronic* state because the $j = 0$ rotational level is of the A_1 representation. For certain excited vibrational or/and electronic states of E and A_2 representations of the ν_3 and ν_4 modes, the $j = 0$ rotational level is allowed.

TABLE 4. The recommended MTCS. The data below 0.65 eV are from the work of Hamilton *et al.*[25] and above 1.5 eV is from the work of Boesten *et al.*[15] Energies are in eV; the cross sections are in units of 10^{-16} cm^{-1}

Electron energy	MTCS	Electron energy	MTCS	Electron energy	MTCS
6.74×10^{-3}	128.5	0.188	19.50	4.78	14.97
7.43×10^{-3}	117.6	0.208	19.15	5.27	14.83
8.20×10^{-3}	107.7	0.229	18.82	5.82	14.63
9.04×10^{-3}	98.80	0.253	18.52	6.41	14.42
9.97×10^{-3}	90.72	0.279	18.23	7.07	14.22
0.0110	83.41	0.308	17.95	7.80	13.30
0.0121	76.80	0.339	17.68	8.61	12.91
0.0134	70.83	0.374	17.42	9.49	13.57
0.0148	65.43	0.413	17.16	10.47	13.20
0.0163	60.56	0.455	16.91	11.55	12.34
0.0179	56.16	0.502	16.65	12.74	11.45
0.0198	52.19	0.554	16.35	14.05	10.73
0.0218	48.61	0.611	15.99	15.49	10.32
0.0241	45.38	0.674	15.60	17.09	10.24
0.0266	42.47	0.743	15.17	18.85	10.13
0.0293	39.85	0.820	14.74	20.79	9.63
0.0323	37.49	0.904	14.31	22.93	9.03
0.0356	35.36	1.00	13.89	25.29	8.48
0.0393	33.46	1.10	13.49	27.89	7.98
0.0434	31.75	1.21	13.12	30.76	7.52
0.0478	30.23	1.34	12.79	33.93	7.24
0.0527	28.88	1.48	12.50	37.42	7.08
0.0582	27.64	1.63	12.30	41.27	6.97
0.0642	26.50	1.79	12.25	45.52	6.83
0.0708	25.50	1.98	12.37	50.21	6.61
0.0780	24.60	2.18	12.69	55.38	6.15
0.0861	23.78	2.41	13.17	61.08	5.76
0.0949	23.05	2.66	13.70	67.36	5.56
0.105	22.38	2.93	14.16	74.30	5.43
0.115	21.78	3.23	14.46	81.95	5.37
0.127	21.24	3.56	14.72	90.38	5.36
0.140	20.74	3.93	14.90	99.69	5.42
0.155	20.29	4.33	14.98	109.95	5.50
0.171	19.88				

The only published data on rotational excitation are a theoretical calculation by Goswami *et al.*,[24] where rotational excitation cross sections starting from $j = 0$ were calculated using the UK R-matrix code and the Quantemol interface.[36] In order to account for transitions starting from a $j = 1$ rotational ground state, we employed a similar procedure using the scattering wave functions of Hamilton *et al.*[25] and, in the outer region, the experimental value for the NF$_3$ dipole moment. Our new data are reproduced in Fig. 6, and numerical values are given in Table 5. The magnitudes of the $\Delta j = 0$ transition cross sections presented here are similar to those calculated by Goswami *et al.*[24] The main differences arise in the region of the two shape resonances. The location of the resonance features in Fig. 6 is in agreement with measured values of Nandi *et al.*[20] at 1.855–1.914 eV; the resonances of Goswami *et al.* are placed higher, at around 4 eV. The dipole-allowed, $\Delta j = 1$ cross sections calculated in this work are larger than those of Goswami *et al.* This is due to the different initial j and subsequent j' states considered. Our $\Delta J > 1$ transition cross sections are of similar magnitude to those calculated by Goswami *et al.*, except when they are affected by the location of the shape resonances.

We also performed a quick calculation to estimate the uncertainty of the obtained cross sections due to parameters of the quantum-chemistry model used. The estimated uncertainty is about 5% for elastic $\Delta j = 0$ transition and about 20% for inelastic transitions.
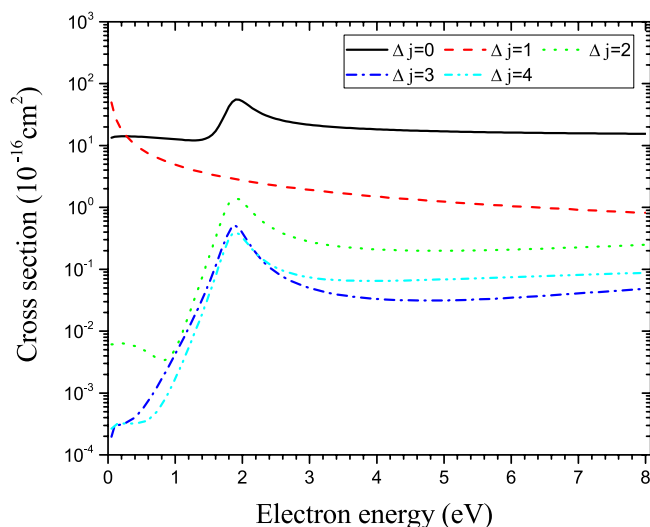

FIG. 6. Rotational excitation cross section from the ground rotational level $j = 1$ to the $j' = 1 - 5$ levels.

TABLE 5. The recommended cross sections for rotational excitation from the ground rotational level $j = 1$ to the $j' = 1 - 5$ levels. Energies are in eV; the cross sections are in units of 10^{-16} cm^{-1}

Electron energy	CS $\Delta j = 0$	CS $\Delta j = 1$	CS $\Delta j = 2$	CS $\Delta j = 3$	CS $\Delta j = 4$
0.05	13.41	49.59	6.115×10^{-3}	1.960×10^{-4}	2.643×10^{-4}
0.10	13.85	30.61	6.176×10^{-3}	3.019×10^{-4}	3.130×10^{-4}
0.15	14.01	22.61	6.293×10^{-3}	3.038×10^{-4}	3.169×10^{-4}
0.20	14.07	18.11	6.325×10^{-3}	3.113×10^{-4}	3.192×10^{-4}
0.25	14.08	15.20	6.275×10^{-3}	3.239×10^{-4}	3.202×10^{-4}
0.30	14.06	13.15	6.155×10^{-3}	3.428×10^{-4}	3.206×10^{-4}
0.35	14.02	11.62	5.974×10^{-3}	3.700×10^{-4}	3.213×10^{-4}
0.40	13.97	10.44	5.740×10^{-3}	4.080×10^{-4}	3.231×10^{-4}
0.45	13.90	9.48	5.462×10^{-3}	4.599×10^{-4}	3.274×10^{-4}
0.50	13.82	8.70	5.149×10^{-3}	5.298×10^{-4}	3.357×10^{-4}
0.55	13.74	8.05	4.813×10^{-3}	6.224×10^{-4}	3.502×10^{-4}
0.60	13.64	7.49	4.467×10^{-3}	7.439×10^{-4}	3.735×10^{-4}
0.65	13.53	7.01	4.128×10^{-3}	9.016×10^{-4}	4.094×10^{-4}
0.70	13.42	6.60	3.820×10^{-3}	1.105×10^{-3}	4.625×10^{-4}
0.75	13.30	6.23	3.572×10^{-3}	1.366×10^{-3}	5.394×10^{-4}
0.80	13.18	5.90	3.422×10^{-3}	1.699×10^{-3}	6.484×10^{-4}
0.85	13.05	5.61	3.423×10^{-3}	2.125×10^{-3}	8.009×10^{-4}
0.90	12.92	5.35	3.642×10^{-3}	2.667×10^{-3}	1.012×10^{-3}
0.95	12.78	5.11	4.173×10^{-3}	3.358×10^{-3}	1.303×10^{-3}
1.00	12.64	4.90	5.142×10^{-3}	4.242×10^{-3}	1.701×10^{-3}
1.05	12.51	4.70	6.719×10^{-3}	5.374×10^{-3}	2.244×10^{-3}
1.10	12.38	4.52	9.142×10^{-3}	6.832×10^{-3}	2.986×10^{-3}
1.15	12.26	4.35	1.274×10^{-2}	8.718×10^{-3}	4.002×10^{-3}
1.20	12.16	4.20	1.799×10^{-2}	1.118×10^{-2}	5.395×10^{-3}
1.25	12.10	4.06	2.554×10^{-2}	1.441×10^{-2}	7.317×10^{-3}
1.30	12.10	3.93	3.637×10^{-2}	1.871×10^{-2}	9.987×10^{-3}
1.40	12.40	3.69	7.420×10^{-2}	3.237×10^{-2}	1.902×10^{-2}
1.50	13.63	3.48	1.533×10^{-1}	5.857×10^{-2}	3.763×10^{-2}
1.60	17.12	3.29	3.218×10^{-1}	1.120×10^{-1}	7.771×10^{-2}
1.70	25.92	3.13	6.627×10^{-1}	2.232×10^{-1}	1.637×10^{-1}
1.80	42.51	2.99	1.160×10^{-00}	4.090×10^{-1}	3.081×10^{-1}
1.85	50.83	2.93	1.343×10^{-00}	4.859×10^{-1}	3.701×10^{-1}
1.90	55.37	2.87	1.404×10^{-00}	5.021×10^{-1}	3.911×10^{-1}
1.95	55.23	2.80	1.349×10^{-00}	4.579×10^{-1}	3.697×10^{-1}
2.00	52.04	2.74	1.226×10^{-00}	3.873×10^{-1}	3.266×10^{-1}
2.05	47.80	2.68	1.083×10^{-00}	3.185×10^{-1}	2.808×10^{-1}
2.10	43.65	2.62	9.487×10^{-1}	2.617×10^{-1}	2.408×10^{-1}
2.20	37.01	2.51	7.369×10^{-1}	1.836×10^{-1}	1.824×10^{-1}
2.30	32.45	2.42	5.942×10^{-1}	1.372×10^{-1}	1.458×10^{-1}
2.40	29.30	2.33	4.978×10^{-1}	1.084×10^{-1}	1.223×10^{-1}
2.50	27.06	2.25	4.306×10^{-1}	8.935×10^{-2}	1.065×10^{-1}
2.60	25.40	2.17	3.822×10^{-1}	7.618×10^{-2}	9.543×10^{-2}
2.70	24.13	2.10	3.461×10^{-1}	6.666×10^{-2}	8.750×10^{-2}
2.80	23.12	2.04	3.185×10^{-1}	5.955×10^{-2}	8.166×10^{-2}
2.90	22.31	1.98	2.969×10^{-1}	5.409×10^{-2}	7.728×10^{-2}
3.00	21.64	1.92	2.796×10^{-1}	4.981×10^{-2}	7.396×10^{-2}
3.50	19.49	1.68	2.302×10^{-1}	3.789×10^{-2}	6.611×10^{-2}
4.00	18.29	1.50	2.095×10^{-1}	3.314×10^{-2}	6.490×10^{-2}
4.50	17.50	1.35	2.010×10^{-1}	3.140×10^{-2}	6.623×10^{-2}
5.00	16.93	1.23	1.993×10^{-1}	3.136×10^{-2}	6.863×10^{-2}
5.50	16.52	1.13	2.020×10^{-1}	3.250×10^{-2}	7.150×10^{-2}
6.00	16.20	1.05	2.079×10^{-1}	3.454×10^{-2}	7.456×10^{-2}
6.50	15.97	0.98	2.161×10^{-1}	3.731×10^{-2}	7.774×10^{-2}
7.00	15.78	0.92	2.260×10^{-1}	4.065×10^{-2}	8.102×10^{-2}
7.50	15.62	0.87	2.369×10^{-1}	4.447×10^{-2}	8.443×10^{-2}
8.00	15.47	0.82	2.484×10^{-1}	4.867×10^{-2}	8.799×10^{-2}

6. Vibrational Excitation Cross Sections

The NF₃ molecule has four vibrational modes, two of which are A_1 non-degenerate modes, ν_1 and ν_2, and the two others, ν_3 and ν_4, are doubly degenerate of E symmetry.[15] The excitation energies of the modes are given in Table 6.

The only available experimental data on vibrational excitation are by Boesten et al.,[15] where DCSs for excitation of the ν_1/ν_3 modes were measured in a crossed-beam experiment. The cross sections obtained are reproduced in Fig. 7. Figure 8 shows the cross section integrated over the solid angle. The corresponding numerical values are

TABLE 6. Vibrational modes and excitation energies of NF_3[15]

Mode	Type	Energy (eV)
ν_1	Symmetric stretch	0.1280
ν_2	Umbrella mode	0.0802
ν_3	Asymmetric stretch	0.1125
ν_4	Asymmetric bend	0.0611

FIG. 7. Experimental DCS for excitation of the ν_1/ν_3 modes.[15] The values for 60°, 70°, etc., are shifted by 0.1, 0.2, etc., units and approach zero at 9 eV.

FIG. 8. Integrated cross section for excitation of the ν_1/ν_3 modes obtained from the data shown in Fig. 7.[15]

TABLE 7. Integrated cross section for vibrational excitation of the ν_1/ν_3 modes.[15] Electron energies are in eV; the cross sections are in units of 10^{-16} cm^{-1}

Electron energy	CS	Electron energy	CS	Electron energy	CS
1.50	1.41	4.07	1.95	6.57	0.44
1.57	1.57	4.14	1.95	6.64	0.43
1.64	1.65	4.20	1.83	6.70	0.41
1.70	1.67	4.27	1.79	6.77	0.39
1.77	1.75	4.34	1.74	6.84	0.39
1.84	1.90	4.41	1.64	6.91	0.39
1.91	1.88	4.47	1.59	6.97	0.38
1.97	1.99	4.54	1.49	7.04	0.36
2.04	2.10	4.61	1.48	7.11	0.35
2.11	2.17	4.68	1.40	7.18	0.33
2.18	2.23	4.74	1.36	7.24	0.33
2.24	2.29	4.81	1.30	7.31	0.32
2.31	2.40	4.88	1.24	7.38	0.30
2.38	2.44	4.95	1.17	7.45	0.30
2.45	2.53	5.01	1.13	7.51	0.30
2.51	2.54	5.08	1.08	7.58	0.29
2.58	2.59	5.15	1.05	7.65	0.29
2.65	2.64	5.22	1.00	7.72	0.28
2.72	2.65	5.28	0.96	7.78	0.27
2.78	2.65	5.35	0.91	7.85	0.28
2.85	2.68	5.42	0.87	7.92	0.27
2.92	2.64	5.49	0.84	7.99	0.26
2.99	2.66	5.55	0.81	8.05	0.25
3.05	2.68	5.62	0.76	8.12	0.24
3.12	2.61	5.69	0.71	8.19	0.23
3.19	2.56	5.76	0.71	8.26	0.23
3.26	2.56	5.82	0.67	8.32	0.24
3.32	2.55	5.89	0.63	8.39	0.24
3.39	2.56	5.96	0.60	8.46	0.24
3.46	2.49	6.03	0.59	8.53	0.25
3.53	2.45	6.09	0.58	8.59	0.24
3.59	2.39	6.16	0.55	8.66	0.23
3.66	2.35	6.23	0.53	8.73	0.21
3.73	2.29	6.30	0.52	8.80	0.21
3.80	2.24	6.36	0.50	8.86	0.22
3.86	2.19	6.43	0.48	8.93	0.21
3.93	2.11	6.50	0.46	9.00	0.20
4.00	2.02				

7. Electron-Impact Electronic Excitation and Dissociation

There are no experimental determinations of electron-impact electronic excitation or dissociation. Theoretically Goswami *et al.*[24] considered inelastic processes in their spherical complex optical potential (SCOP) calculations, but this procedure does not separate these into their individual contributions. Here we therefore concentrate on the recent R-matrix calculation[37] by Hamilton *et al.*[25] and older Kohn calculations by Rescigno.[22] Both calculations are based on the use of a close-coupling expansion of the target wave functions.

Electron-impact dissociation reactions go via excitation to electronically excited states of the target which then dissociate.[38] The dissociation of the N–F in NF_3 is 2.52 eV,[39,40] and no low-lying metastable electronically excited states of NF_3 are known. It can therefore be assumed that all electronic excitation leads to dissociation; a similar

given in Table 7. Because the DCS was not measured for angles below 20° and above 130°, performing the integration, we assumed that the DCS below 20° is equal to the one at 20° and the DCS above 130° is equal to the one at 130°. Such an assumption introduces a significant uncertainty, of the order of 30%, into the integrated cross section. Note that the present estimate of the vibrational cross section at 2.5 eV maximum agrees with the value used by Lisovskiy *et al.*[26] for modeling electron transport coefficients in NF_3.

assumption has been made in cases where the results are testable against experiment[41] and has been found to be reasonable. Both Rescigno and Hamilton *et al.* made this assumption for NF$_3$.

For an accurate calculation of these processes, a large number of electronically excited states need to be considered. Born corrections to the electron-impact excitation cross sections were used to account for long range dipole effects.[42,43]

Hamilton *et al.*[25] estimated the products of the dissociation process by analogy with the observed photodissociation cross sections of Seccombe *et al.*[44] which suggested that the following process can occur:

$$\mathrm{NF_3}(a\,^1E) \rightarrow \mathrm{NF}(b\,^1\Sigma^+) + \mathrm{F_2}, \quad (2)$$

$$\mathrm{NF_3}(b\,^1A_1) \rightarrow \mathrm{NF_2}(A\,^2A_1) + \mathrm{F}(^2P_u), \quad (3)$$

$$\mathrm{NF_3}(c\,^1A_2) \rightarrow \mathrm{NF_2}(B\,^2A_1) + \mathrm{F}(^2P_u), \quad (4)$$

$$\mathrm{NF_3}(d\,^1E) \rightarrow \mathrm{NF_2}(C\,^2B_2) + \mathrm{F}(^2P_u), \quad (5)$$

$$\mathrm{NF_3}(A\,^3E) \rightarrow \mathrm{NF}(b\,^1\Sigma^+) + \mathrm{F_2}, \quad (6)$$

$$\mathrm{NF_3}(A\,^3E) \rightarrow \mathrm{NF}(B\,^3\Sigma^+) + \mathrm{F_2}, \quad (7)$$

$$\mathrm{NF_3}(B\,^3A_1) \rightarrow \mathrm{NF_2}(A\,^2A_1) + \mathrm{F}(^2P_u), \quad (8)$$

$$\mathrm{NF_3}(B\,^3A_1) \rightarrow \mathrm{NF_2}(a\,^4A_1) + \mathrm{F}(^2P_u), \quad (9)$$

$$\mathrm{NF_3}(C\,^3A_2) \rightarrow \mathrm{NF_2}(B\,^2A_1) + \mathrm{F}(^2P_u), \quad (10)$$

$$\mathrm{NF_3}(C\,^3A_2) \rightarrow \mathrm{NF_2}(b\,^4A_1) + \mathrm{F}(^2P_u), \quad (11)$$

$$\mathrm{NF_3}(D\,^3E) \rightarrow \mathrm{NF_2}(C\,^2B_2) + \mathrm{F}(^2P_u), \quad (12)$$

$$\mathrm{NF_3}(D\,^3E) \rightarrow \mathrm{NF_2}(c\,^4B_2) + \mathrm{F}(^2P_u). \quad (13)$$
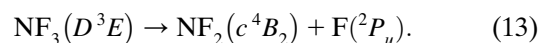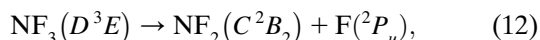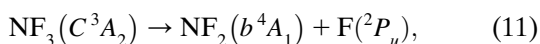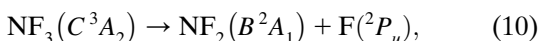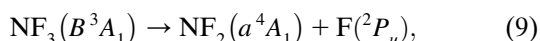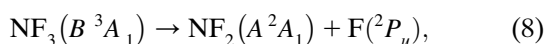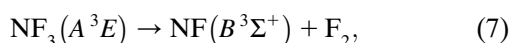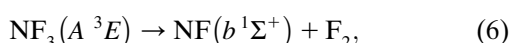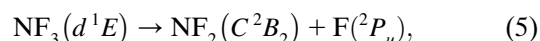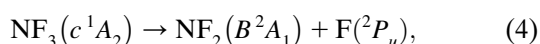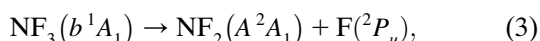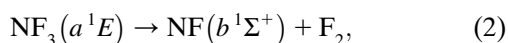
These results, which are given in Fig. 9 and Table 8, are the best ones currently available, but they must be considered to be estimates. Experimental studies of electron-impact dissociation of NF$_3$ would be very useful.
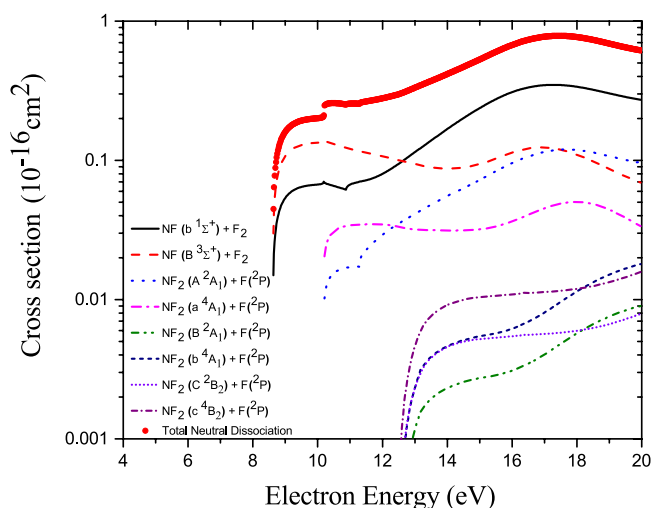

FIG. 9. Cross sections for electron-impact dissociation into various channels, taken from the recent R-matrix calculation by Hamilton *et al.*[25]

8. Ionization Cross Section

NF$_3$ ionization was measured in several experiments and calculated in the Binary Encounter Bethe (BEB) model developed by Kim and Rudd.[45] Generally, the agreement between experiments and the theory is rather poor: experimental data are lower than values calculated. Recommended values from the Landolt-Börnstein review[46] were obtained as averages of Tarnovsky *et al.*[47] and Haaland *et al.*[17] Total and partial ionization (into NF$_3^+$, NF$_2^+$, NF$^+$, N$^+$, NF$_3^{2+}$, NF$_2^{2+}$, and NF^{2+}) cross sections were compiled between 14 and 200 eV. No data were reported of F$^+$ due to a serious disagreement between the two experiments. (Note that the figure in L-B is mislabeled.) In Fig. 10, we compare the recommended values from the L-B review that resumed earlier experiments, with the recent measurements of Rahman *et al.*[18]

Tarnovsky *et al.*[16] measured total and partial cross sections in two laboratories (using a magnetic selector and a fast-beam method). The agreement for the NF$_3^+$ parent ionization from the two laboratories is within 8%. Partial cross sections for NF$_2^+$, NF$^+$, and F$^+$ ions were measured by the fast ion beam method. An upper limit for the formation of N$^+$ was also determined. Total declared uncertainties on cross sections were ±20%.

Haaland *et al.*[17] used a modified Fourier-transform mass spectrometry: ions were confined radially by a high (2T) magnetic field and axially by an electrostatic (1–2 V) potential. In this method, no ions are actually collected, but, instead, their electromagnetic influence on the antenna is recorded. Cross sections were normalized to Ar ionization cross sections of Wetzel;[48] the uncertainty of this normalization is ±12%,[17] and the declared total uncertainty is ±16%. Data for all partial processes, including double ionizations (NF$_3^{2+}$, NF$_2^{2+}$, and NF^{2+}), were reported up to 200 eV.

Rahman *et al.*[18] measured total and partial (but only for single ionization) cross sections up to 500 eV. They used a time-of-flight (TOF) spectrometer with a 30 cm-long free-flight path for ions. They normalized relative data to the Ar$^+$ ionization cross section at 100 eV of Krishnakumar and Srivastava.[49] The declared total uncertainty was ±15%.

The best agreement (within some 15% up to 100 eV) between the three experiments[16–18] is seen for the NF$_3^+$ parent ion; at higher energies, data of Rahman *et al.*[18] and Tarnovsky *et al.*[16] still agree within 10%, while results of Haaland *et al.* are somewhat (30% at 200 eV) higher. For NF$_2^+$, the measurements of Rahman *et al.* agree very well (within 10%) with those by Haaland *et al.*, but those of Tarnovsky *et al.* are by 30% lower at 200 eV. In turn, for the NF$^+$ ion, the data of Haaland are somewhat lower (20% at 100 eV) than the two other sets considered here. Note from Fig. 10 that the experiment of Rahman *et al.* tends to produce higher cross sections for NF$_2^+$ and NF$^+$ ions than the recommended data from the Landolt-Börnstein[46] review; the same holds for the total ionization.

For light ions (N$^+$ and F$^+$), the results of Haaland *et al.*[17] are systematically lower (by a factor of about 10 for F$^+$ and 50 for N$^+$) than the data by Rahman *et al.*[18] The upper limits for N$^+$ and F$^+$ at 100 eV given by Tarnovsky *et al.*[16] (0.1×10^{-16}

TABLE 8. Cross sections for electron-impact dissociation calculated by Hamilton *et al.*;[25] the products of the dissociation process were estimated by analogy with the observed photodissociation cross sections of Seccombe *et al.*[44]

Energy (eV)	Neutral dissociation (10^{-16} cm^2)	NF + F$_2$ (10^{-16} cm^2)	NF$_2$ + F (10^{-16} cm^2)	Energy (eV)	Neutral dissociation (10^{-16} cm^2)	NF + F$_2$ (10^{-16} cm^2)	NF$_2$ + F (10^{-16} cm^2)
8.63	0.044 87	0.044 87		10.91	0.254 51	0.186 56	0.050 96
8.74	0.110 03	0.110 03		10.95	0.255 55	0.187 35	0.051 15
8.86	0.139 13	0.14		10.99	0.256 05	0.187 63	0.051 31
8.97	0.157 67	0.16		11.01	0.256 2	0.187 69	0.051 38
9.09	0.170 47	0.17		11.05	0.256 36	0.187 68	0.051 51
9.20	0.179 63	0.18		11.09	0.256 4	0.187 58	0.051 61
9.32	0.186 27	0.19		11.11	0.256 38	0.187 51	0.051 66
9.43	0.191 11	0.19		11.15	0.256 3	0.187 32	0.051 73
9.54	0.194 59	0.19		11.19	0.256 16	0.187 11	0.051 78
9.66	0.197 07	0.20		11.21	0.256 07	0.187 01	0.051 8
9.77	0.198 84	0.20		11.25	0.255 87	0.186 8	0.051 81
9.89	0.200 12	0.20		11.27	0.255 75	0.186 7	0.051 79
10.00	0.201 25	0.20		11.29	0.255 6	0.186 63	0.051 73
10.01	0.201 36	0.201 36		11.31	0.259 13	0.186 76	0.053 32
10.05	0.201 86	0.201 86		11.35	0.261 74	0.186 36	0.054 95
10.09	0.202 52	0.202 52		11.39	0.263 03	0.186 12	0.055 75
10.11	0.202 96	0.202 96		11.41	0.263 59	0.186 02	0.056 1
10.15	0.204 39	0.204 39		11.45	0.264 63	0.185 82	0.056 75
10.17	0.205 83	0.205 83		11.49	0.265 62	0.185 66	0.057 35
10.19	0.210 64	0.210 64		11.50	0.265 87	0.185 62	0.057 5
10.21	0.248 34	0.207 52	0.030 62	11.89	0.276 28	0.186 05	0.062 49
10.23	0.250 86	0.205 95	0.033 68	12.27	0.289 8	0.190 53	0.066 71
10.25	0.252 71	0.204 93	0.035 83	12.66	0.308 96	0.198 43	0.073 5
10.29	0.255 21	0.203 32	0.038 92	13.05	0.337 06	0.210 21	0.084 97
10.31	0.256 08	0.202 6	0.040 11	13.43	0.367 43	0.224 96	0.095 35
10.35	0.257 31	0.201 25	0.042 05	13.82	0.400 73	0.244 45	0.103 66
10.39	0.258 05	0.199 94	0.043 58	14.20	0.438 73	0.268 77	0.111 44
10.41	0.258 28	0.199 3	0.044 24	14.59	0.481 14	0.297 35	0.119 12
10.45	0.258 53	0.198 03	0.045 37	14.98	0.529 12	0.329 51	0.127 68
10.49	0.258 54	0.196 78	0.046 32	15.36	0.583 34	0.365 12	0.137 8
10.51	0.258 47	0.196 15	0.046 74	15.75	0.640 31	0.401 23	0.149 51
10.55	0.258 22	0.194 91	0.047 48	16.14	0.694 57	0.433 12	0.162 53
10.59	0.257 84	0.193 68	0.048 12	16.52	0.738 77	0.456 73	0.175 08
10.61	0.257 61	0.193 07	0.048 4	16.91	0.770 05	0.469 28	0.186 98
10.65	0.257 06	0.191 85	0.048 91	17.30	0.785 05	0.470 31	0.196 54
10.69	0.256 43	0.190 63	0.049 35	17.68	0.783 14	0.461 11	0.202 38
10.71	0.256 08	0.190 02	0.049 54	18.07	0.766 3	0.444 14	0.203 96
10.75	0.255 32	0.188 8	0.049 89	18.45	0.738 6	0.422 44	0.201 68
10.79	0.254 48	0.187 55	0.050 2	18.84	0.705 16	0.399 07	0.196 65
10.81	0.254 02	0.186 9	0.050 34	19.23	0.671 13	0.376 57	0.190 45
10.85	0.252 98	0.185 54	0.050 59	19.61	0.640 66	0.356 69	0.184 59
10.87	0.252 33	0.184 73	0.050 7	20.00	0.616 6	0.340 47	0.180 21
10.89	0.253 35	0.185 55	0.050 84				

and 0.3 × 10^{-16} cm^2, respectively) roughly agree with measurements by Rahman *et al.*; see Fig. 10. Some possible systematic errors are related to the experimental methods used. In the experiment of Haaland *et al.*,[17] this is the indirect measurement of the signal from ions, clearly making the determination of partial cross sections for light ions such as N$^+$ and F$^+$ uncertain (i.e., lighter than Ar$^+$ used for normalization). On the other hand, this is the only experiment sufficiently sensitive to detect doubly charged molecular fragments, NF$_3^{2+}$, NF$_2^{2+}$, and NF^{2+}, with cross sections of the order 10^{-20} − 10^{-19} cm^2; see Table 9.

Another question is the dependence of the experimental sensitivity on the collision energy. The ion optics performs some focusing, and the efficiency of ion collection can depend on their post-collisional velocities. As it was discussed for a long time in CF$_4$, see Ref. 50, the problem is particularly

difficult when ions are formed with high velocities and through different fragmentation channels. For NF$_3$, Tarnovsky *et al.*[16] observed that NF$_2^+$ ions are formed with little excess kinetic energy for impact energies near the threshold, but NF$^+$ ions appear with a broad distribution of excess kinetic energy, ranging from zero to about 4 eV.

In the TOF method, some metastable ions can decay before reaching the detector. A rough evaluation of flight times for heavier ions gives values in the microsecond range—long enough for some fragmentation to occur. This, tentatively, would explain lower values of the NF$_2^+$ cross section up to about 40 eV in the experiment of Rahman *et al.* as compared to the Landolt-Börnstein values; see Fig. 10. In turn, cross sections for N$^+$ and F$^+$ show some unusual enhancement in this energy region, which would indicate some in-flight decay of heavier (NF$_2^+$ and NF$^+$) ions; see Fig. 10.
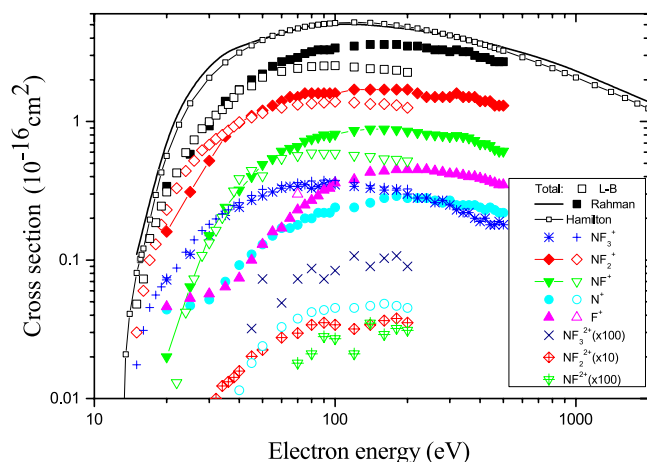
FIG. 10. Comparison of the compilation[46] of earlier experiments with the recent measurements by Rahman *et al.*[18] Closed symbols (squares, stars, diamonds, inverted triangles, circles, and triangles) are the data of Rahman *et al.* (for total ionization and production of NF$_3^+$, NF$_2^+$, NF$^+$, N$^+$ and F$^+$ ions, respectively). Open symbols for NF$_3^+$, NF$_2^+$, and NF$^+$ are from the Landolt-Börnstein compilation;[46] an open circle and an open triangle are upper limits for N$^+$ and F$^+$ production, respectively, from the experiment of Tarnovsky *et al.*.[16] Crossed symbols (x, diamonds, inverted triangles) are L-B recommended values for doubly charged ions (NF$_3^{2+}$, NF$_2^{2+}$, and NF$^+$, respectively)—the data are based on measurements by Haaland *et al.*[17] (note the multiplying factors in the figure). Thick black line is the total ionization in the complex-potential optical model by Rahman *et al.*;[18] thin black line with squares is the total ionization in the BEB model by Hamilton *et al.*[25]

TABLE 9. Ionization cross sections for formation of doubly charged ions, from the Landolt-Börnstein review[46] (based on Haaland *et al.*[17]) data. Cross sections are in 10^{-18} cm^2 units. The overall uncertainty is ±50%

Energy (eV)	NF$_3^{2+}$ (10^{-18} cm^2)	NF$_2^{2+}$ (10^{-18} cm^2)	NF^{2+} (10^{-18} cm^2)
30	...	0.0589	...
32	...	0.0998	...
34	...	0.123	...
36	...	0.132	...
38	...	0.142	...
40	...	0.158	...
45	0.032	0.201	...
50	0.073	0.224	...
60	0.049	0.276	0.000
70	0.073	0.296	0.018
80	0.087	0.341	0.021
90	0.073	0.353	0.028
100	0.084	0.341	0.027
120	0.107	0.318	0.021
140	0.090	0.341	0.035
160	0.103	0.366	0.029
180	0.107	0.379	0.032
200	0.090	0.353	0.031

8.1. BEB model

The BEB model was employed by Huo *et al.*,[51] Haaland *et al.*,[17] and Szmytkowski *et al.*[14] to calculate the ionization cross section of NF$_3$—all giving the maximum for the total ionization cross section of about 4.8×10^{-16} cm^2. This also agrees with the "rule-of-thumb" noticed recently for the CH$_4$, CH$_3$F, . . . , CF$_4$ series[52] that the maximum in the total ionization cross section (in 10^{-16} cm^2) can be estimated as $4/3\alpha$,

where the dipole polarizability α of the molecule is expressed in 10^{30} m^3 units. Using for NF$_3$ the dipole polarizability of 3.62×10^{-30} m^3 from Ref. 29, one gets a maximum of the total ionization cross section of 4.84×10^{-16} cm^2. Recently, Hamilton *et al.*[25] calculated BEB ionization cross sections using Dunning's augmented Gaussian-type orbitals (aug-cc-pVTZ GTO) and obtained a somewhat higher TCS maximum (5.19×10^{-16} cm^2). Subsequently, they applied the same BEB-like analytical expression to derive partial ionization cross sections, adapting appropriate threshold energies. Relative amplitudes were deduced from the NIST (National Institute of Standards and Technology)[27] electron-impact ionization mass spectrum at 100 eV. Results for the TCS are shown in Fig. 10 and for partial cross sections are shown in Fig. 11. We also adopt these cross sections as recommended values; see Table 11. We also note that the BEB TCS agrees very well with the optical complex-potential calculation by Rahman *et al.*;[18] see Fig. 10.

Figure 11 compares BEB[25] partial cross sections with the normalized partial cross sections of Rahman *et al.* To do this normalization, the sum of experimental partial cross sections at every energy has been normalized to the BEB value; subsequently at this energy, all partial cross sections have been multiplied by the factor obtained. The normalization factors range from 2.3 at 25 eV to 1.22 at 500 eV.

This comparison allows one to distinguish the difference between the expected partial cross sections and those actually measured in the TOF experiment. The NF$_2^+$ experimental signal in the energy range above 50 eV is systematically lower than that of the BEB model; the same holds for the NF$_3^+$ ion which was measured (in all three[16–18] experiments) to be roughly half as abundant as the BEB[25] values (that were obtained, we recall, via the NIST mass spectrum). Figure 11 visualizes that the deficits in the NF$_3^+$ and NF$_2^+$ experimental abundances are compensated by higher values of F$^+$, NF$^+$, and N$^+$ signals. This once again indicates some complex mechanisms of the dissociative ionization.
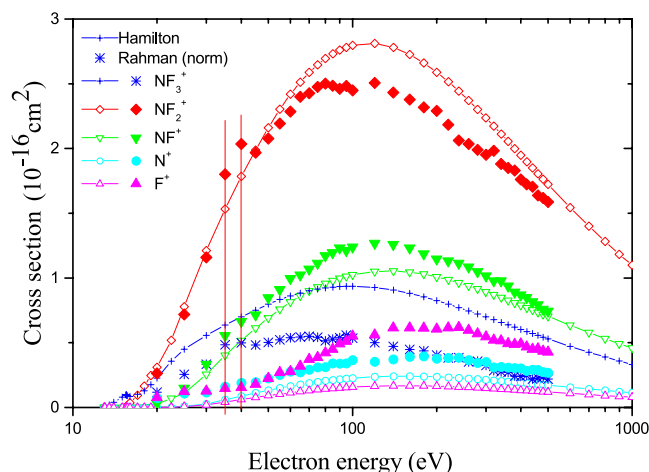

FIG. 11. Comparison of BEB-like partial cross sections by Hamilton *et al.*[25] with measurements of Rahman *et al.*[18] The latter partial cross sections (the sum of them) have been normalized, at each energy, to the BEB[25] total ionization cross section. Vertical lines (34.6 eV and 40.4 eV) show thresholds for (F$^+$ + NF$^+$ + F) and (F$^+$ + N$^+$ + 2F) channels.

TABLE 10. Threshold energy values (in eV) for various fragments observed and their comparison with earlier measurements. Observed thresholds are shown against the estimated ones, wherever possible

Ions	Channel	ΔH^o	Rahman *et al.*[18]	Reese *et al.*[53]	Tarnovsky *et al.*[16]
NF_3^+	$NF_3 \rightarrow NF_3^+$	13.5	13.5 ± 0.6	13.2 ± 0.2	13.6 ± 0.2
NF_2^+	$NF_3 \rightarrow NF_2^+ + F$	14.0	14.5 ± 0.6	14.2 ± 0.3	14.5 ± 0.4
	$\rightarrow NF_2^+ + F^-$	10.4	. . .	. . .	. . .
	. . .	. . .	16 ± 0.6	. . .	. . .
NF^+	$NF_3 \rightarrow NF^+ + 2F$	17.45	17.5 ± 0.7	17.9 ± 0.3	17.6 ± 0.4
	$\rightarrow NF^+ + F_2^-$	14.45	. . .	. . .	. . .
	$\rightarrow NF^+ + F + F^-$	13.85	. . .	. . .	. . .
	$\rightarrow NF^+ + F^+ + F$	34.6	. . .	. . .	. . .
	. . .	. . .	20 ± 0.7	. . .	. . .
F^+	$NF_3 \rightarrow F^+ + NF_2^-$	18.8	19 ± 1	. . .	. . .
	$\rightarrow NF + F^+ + F$	22.0	. . .	. . .	. . .
	$\rightarrow N + 2F + F^+$	25.85	25 ± 1	25 ± 1	. . .
	$\rightarrow F^+ + NF^+ + F$	34.6	33 ± 1	. . .	36
	$\rightarrow F^+ + N^+ + 2F$	40.4	. . .	. . .	. . .
N^+	$NF_3 \rightarrow N^+ + 3F$	23.0	22 ± 1	22.2 ± 0.2	. . .
	$\rightarrow N^+ + F + F_2^-$	20.0	. . .	. . .	. . .
	$\rightarrow N^+ + F^- + F_2$	19.4	. . .	. . .	. . .

8.2. Dissociative ionization channels

Ionization thresholds were thoroughly reported by Rahman *et al.*[18] and Tarnovsky *et al.*[16] The threshold for NF_3^+ parent ion is 13.6±0.2 eV.[16] The NF_2^+ ion shows, according to Rahman *et al.*, two onsets that are closely spaced (14.5 and 16 eV); note that only one value (14.5 ± 0.4 eV[16]) was reported by other experiments; see Table 10. Three onsets were identified by Tarnovsky *et al.* for the NF^+ ion: (NF^+ + 2F) at 17.6 eV, (F^+ + NF^+ + F) at 36.5 eV (reported by Rahman

et al.[18] in the F^+ production channel), and another, not identified, at 21.8 eV; see Table 3. Rahman *et al.* reported a threshold of 19 ± 1 eV for F^+ production and assigned it to the $NF_3 \rightarrow F^+ + NF_2^-$ process. Note that this is the only report on the dipolar dissociation in NF_3.

8.3. Recommended values

Taking into account the significant differences between experiments (and their different sensitivities), we decided to

TABLE 11. Recommended ionization cross sections for NF_3: BEB values from Ref. 25; see text. Energies are in eV, and cross sections are in 10^{-16} cm^2 units. The overall uncertainty is ±10% for TCSs and ±20% for partial ones

Energy	N^+	F^+	NF^+	NF_2^+	NF_3^+	Total	Energy	N^+	F^+	NF^+	NF_2^+	NF_3^+	Total
14	. . .	. . .	. . .	. . .	0.04	0.04	200	0.24	0.16	1.01	2.59	0.83	4.83
15	. . .	. . .	. . .	. . .	0.08	0.08	220	0.23	0.16	0.99	2.52	0.80	4.69
16	. . .	. . .	. . .	0.04	0.09	0.12	240	0.23	0.16	0.96	2.44	0.77	4.56
17	. . .	. . .	. . .	0.10	0.10	0.20	260	0.22	0.16	0.94	2.37	0.75	4.44
18	. . .	. . .	. . .	0.17	0.13	0.30	280	0.22	0.15	0.92	2.30	0.72	4.31
19	. . .	. . .	0.01	0.25	0.18	0.43	300	0.21	0.15	0.89	2.24	0.70	4.19
20	. . .		0.03	0.31	0.23	0.56	320	0.21	0.15	0.87	2.17	0.68	4.08
25	0.01	0.01	0.11	0.78	0.45	1.35	340	0.21	0.14	0.85	2.11	0.66	3.96
30	0.03	0.02	0.26	1.21	0.56	2.07	360	0.20	0.14	0.83	2.06	0.64	3.86
35	0.06	0.04	0.40	1.53	0.64	2.67	380	0.20	0.14	0.81	2.00	0.62	3.76
40	0.09	0.06	0.52	1.79	0.70	3.15	400	0.19	0.13	0.79	1.95	0.60	3.66
45	0.11	0.08	0.61	1.99	0.75	3.54	420	0.19	0.13	0.77	1.90	0.59	3.57
50	0.13	0.09	0.69	2.16	0.80	3.88	440	0.18	0.13	0.75	1.85	0.57	3.48
55	0.15	0.1	0.76	2.30	0.83	4.15	460	0.18	0.12	0.74	1.81	0.56	3.40
60	0.17	0.11	0.81	2.42	0.86	4.38	480	0.18	0.12	0.72	1.76	0.54	3.32
65	0.18	0.12	0.86	2.51	0.88	4.56	500	0.17	0.12	0.70	1.72	0.53	3.25
70	0.19	0.13	0.90	2.59	0.90	4.71	600	0.16	0.11	0.64	1.54	0.47	2.92
75	0.20	0.14	0.93	2.65	0.91	4.83	700	0.14	0.10	0.58	1.40	0.43	2.65
80	0.21	0.14	0.96	2.69	0.92	4.93	800	0.13	0.09	0.53	1.28	0.39	2.43
85	0.21	0.15	0.98	2.73	0.93	5.00	900	0.12	0.09	0.49	1.18	0.36	2.24
90	0.22	0.15	1.00	2.76	0.93	5.06	1000	0.11	0.08	0.46	1.10	0.33	2.08
95	0.22	0.16	1.01	2.78	0.94	5.11	1200	0.10	0.07	0.40	0.96	0.29	1.83
100	0.23	0.16	1.03	2.80	0.94	5.14	1400	0.09	0.06	0.36	0.86	0.26	1.63
120	0.24	0.16	1.05	2.81	0.93	5.19	1600	0.08	0.06	0.33	0.78	0.23	1.48
140	0.24	0.17	1.05	2.78	0.91	5.15	1800	0.08	0.05	0.30	0.71	0.21	1.35
160	0.24	0.17	1.05	2.73	0.88	5.06	2000	0.07	0.05	0.28	0.66	0.20	1.25
180	0.24	0.17	1.03	2.66	0.85	4.95							

recommend total and partial ionization cross sections from the recent BEB analysis by Hamilton et al.,[25] detailed results of which are given in Table 11. We stress that such a choice is not free of some coarse assumptions: the validity of the BEB model for partial cross sections and correct procedures in measurements of partial ions in the NIST experiment. We are also aware that our explanations for the differences between the most recent[18] and earlier experiments[16,17] are only tentative. Therefore, we refer the reader to data by Rahman et al.[18] (Table 2 in their paper) as a complementary choice. In view of importance of NF$_3$ for plasma processes in semiconductor industries, verification of cross sections for total and partial ionization is urgent; new theories would be also welcome. The estimated uncertainty on presently recommended values is +10%–20% for the total ionization and +20%–30% for partial cross sections.

9. DEA Cross Section

There are only two published reports, relevant to this evaluation purpose, on the absolute measurements of the DEA cross sections for NF$_3$: Harland and Franklin[19] and Nandi et al.[20] Other than these, Chantry reported the DEA cross sections for NF$_3$ at a conference and the results were also contained in a book[21] but were not published in a journal, and therefore, this will not be discussed any further here. There are two experimental determinations of the electron attachment coefficient in swarms,[54,55] but the two results are not consistent with each other and it is unclear which is more reliable. Harland and Franklin[19] employed a linear TOF mass spectrometer to measure translational energies of negative ions formed by dissociative resonance capture processes from NF$_3$. Nandi et al.[20] have pointed out that mass to charge ratio analysis becomes imperative for the measurement of partial cross sections when more than one type of ions are produced, and then it is necessary that the extraction, mass analysis, and the detection procedures for these ions are carried out without discriminating against their initial kinetic energies, angular distributions, or their mass to charge ratios. These necessitated them to use a crossed-beam geometry, and an efficient solution to these problems was to use a segmented TOF mass spectrometer along with the pulsed-electron-beam and pulsed-ion-extraction techniques and the relative flow technique. The results of Harland and Franklin[19] and Nandi et al.[20] agree well with each other in the positions of the resonance peaks, but the magnitude shows the differences as nearly big as a factor of four. For example, the cross sections of the formation of F$^-$ are 0.6×10^{-16} cm^2 for Harland and Franklin and 2.2×10^{-16} cm^2 for Nandi et al. In both experiments, F$^-$ is the most dominant ion from the DEA process with very small intensities of F$_2^-$ and NF$_2^-$. For F$_2^-$, the cross section of Nandi et al. is smaller than that obtained by Harland and Franklin. For NF$_2^-$, the cross section of Nandi et al. is larger than the corresponding data of Harland and Franklin within a factor of 2. For all the ions, there is a finite cross section even at zero energy. The electron beam has a half-width of 0.5 eV. It is possible that the high energy tail of the

TABLE 12. Recommended dissociative attachment cross sections for the formation of F$^-$, F$_2^-$, and NF$_2^-$ from NF$_3$.[20] The uncertainties are estimated to be about 15%

Energy (eV)	$\sigma(F^-)$ (10^{-16} cm^2)	$\sigma(F_2^-)$ (10^{-19} cm^2)	$\sigma(NF_2^-)$ (10^{-20} cm^2)
0.0	0.53	0.18	0.48
0.1	0.58	0.23	0.34
0.2	0.64	0.30	0.38
0.3	0.72	0.34	0.41
0.4	0.79	0.35	0.46
0.5	0.92	0.38	0.50
0.6	1.04	0.48	0.47
0.7	1.21	0.51	0.67
0.8	1.33	0.63	0.71
0.9	1.52	0.71	0.93
1.0	1.68	0.82	1.17
1.3	2.03	1.15	2.20
1.5	2.16	1.40	3.34
1.7	2.20	1.60	4.50
1.9	2.14	1.59	4.93
2.0	2.08	1.65	4.62
2.4	1.74	1.31	2.68
2.8	1.28	0.87	1.06
3.2	0.84	0.50	0.50
3.6	0.50	0.28	0.29
4.0	0.28	0.15	0.11
4.4	0.14	0.07	0.09
4.8	0.07	0.03	0.03
5.0	0.04	0.02	0.01
5.1	0.04	0.02	0.03
5.2	0.03	0.02	0.06
5.3	0.02	0.01	0.05
5.4	0.02	0.01	0.05
5.5	0.02	0.01	0.06
5.6	0.01	0.01	0.07
5.7	0.01	0.01	0.06
5.8	0.01	0.01	0.06
5.9	0.01	0.01	0.07
6.0	0.01	0.01	0.03

electron energy distribution is giving rise to the finite cross section at zero energy for F$_2^-$ and NF$_2^-$.[20] The high resolution measurements of Ruckhaberle et al.[56] showed a finite cross section for F$^-$ at zero energy, whereas both F$_2^-$ and NF$_2^-$ appear only above 1 eV.[20] Considering the fact that Nandi et al. have made more complete measurements of the experimental parameters, we recommend their cross sections for the DEA process of NF$_3$. Complete numerical values of the recommended cross sections are presented in Table 12 and Fig. 12. Nandi et al. estimated the uncertainty to be about 15%.

10. Summary and Future work

We present a systematic review of the published cross sections for processes resulting from electron collisions with NF$_3$ until end of 2016. Both measurements and theoretical predictions are considered, although priority is given to high quality measurements with published uncertainties where available. The summary of the cross section for electron collisions with NF$_3$ is given in Fig. 13. There is considerable variation in the reliability of the available data. For the TCS, the MTCS, and the ionization cross section, it is possible to recommend values over an extended energy range with small
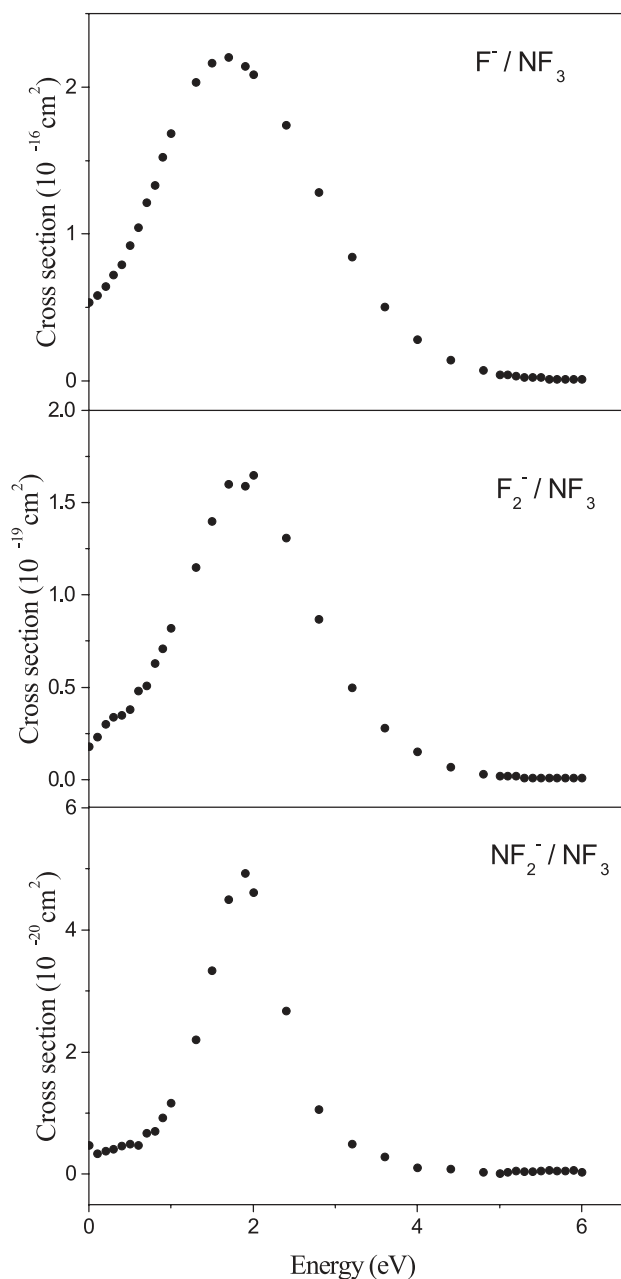
FIG. 12. Recommended cross sections for the formation of F^-, F_2^-, and NF_2^- from NF_3. Note the different scales in cross sections.[20]

FIG. 13. The summary of the cross section for electron collisions with NF_3. TCS—total scattering, ES—elastic scattering, MT—momentum transfer, ION—partial ionization, TICS—total ionization, VI—vibrational excitation, RO—rotational excitation, DEA—dissociative electron attachment, DISS—neutral dissociation cross section.

recommend using the most recent experimental data and are able to provide the estimated uncertainty to be about 15%.

This evaluation is one in a series of systematic evaluations[33,57] of electron collision processes for key molecular targets. Other evaluations will appear in future papers.

Acknowledgments

11. References

[1]S. Huang, V. Volynets, J. R. Hamilton, S. Lee, I.-C. Song, S. Lu, J. Tennyson, and M. J. Kushner, "Insights to scaling remote plasma sources sustained in NF_3 mixtures," J. Vac. Sci. Technol., A **35**, 031302 (2017).

[2]L. Pruette, S. Karecki, R. Chatterjee, R. Reif, T. Sparks, and V. Vartanian, "High density plasma oxide etching using nitrogen trifluoride and acetylene," J. Vac. Sci. Technol., A **18**, 2749–2758 (2000).

[3]J. M. Veilleux, M. S. El-Genk, E. P. Chamberlin, C. Munson, and J. FitzPatrick, "Etching of UO_2 in NF_3 RF plasma glow discharge," J. Nucl. Mater. **277**, 315–324 (2000).

[4]G. Bruno, P. Capezzuto, G. Cicala, and P. Manodoro, "Study of the NF_3 plasma cleaning of reactors for amorphous-silicon deposition," J. Vac. Sci. Technol., A **12**, 690–698 (1994).

[5]B. E. E. Kastenmeier, P. J. Matsuo, G. S. Oehrlein, and J. G. Langan, "Remote plasma etching of silicon nitride and silicon dioxide using NF_3/O_2 gas mixtures," J. Vac. Sci. Technol., A **16**, 2047–2056 (1998).

[6]F. H. C. Goh, S. M. Tan, K. Ng, H. A. Naseem, W. D. Brown, and A. M. Hermann, in *Amorphous Silicon*, edited by P. C. Taylor, M. J. Thompson, P. G. Lecomber, Y. Hamakaura, and A. Madan (MRS, Pittsburgh, PA 1990), pp. 75–80.

uncertainties, typically 10%–15%. The situation is significantly worse for other processes. For electron-impact rotational excitation, we rely on predictions from *ab initial* calculations, but these calculations are far from being complete. The experimental work on this process would be welcome. There is one direct experimental measurement of electron-impact vibrational excitation cross sections. Theoretical treatments of this process are possible and should be performed by theorists. Some new, reliable beam measurements of this process would be very helpful. Electron-impact dissociation is an important process, but the available measurements are inconsistent with each other, and we are unable to recommend a good set of data for this process. A new study on the problem is needed. Finally there are two data available for the DEA process. Here we
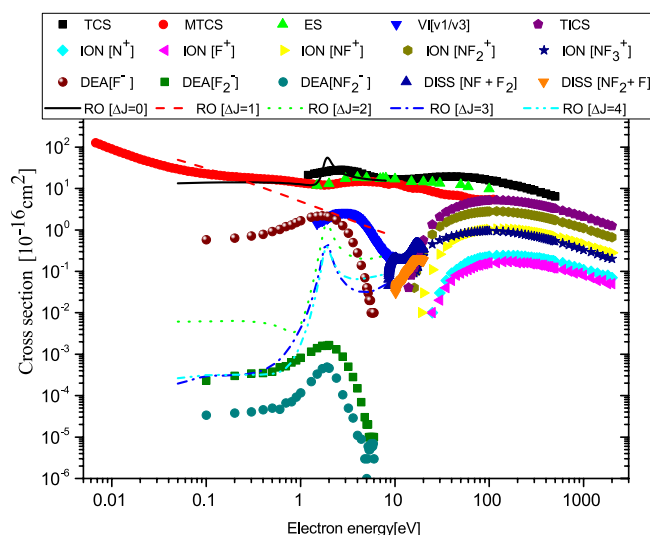
[7]S. Kurtz, R. Reedy, B. Keyes, G. Barber, J. Geisz, D. Friedman, W. McMahon, and J. Olson, "Evaluation of NF$_3$ versus dimethylhydrazine as N sources for GaAsN," J. Crystal Growth **234**, 323–326 (2002).

[8]J. B. Park, J. S. Oh, E. Gil, S.-J. Kyoung, J.-S. Kim, and G. Y. Yeom, "Plasma texturing of multicrystalline silicon for solar cell using remote-type pin-to-plate dielectric barrier discharge," J. Phys. D: Appl. Phys. **42**, 215201 (2009).

[9]J. Gao, H. Zhu, Y. Wang, Z. Wang, F. Guan, J. Ni, J. Yin, L. Lan, Y. Bai, Y. Ma, Y. Mai, M. Wan, and Y. Huang, "Improvement of a-Si:H solar cell performance by SiH$_4$ purging treatment," Vacuum **89**, 7–11 (2013).

[10]M. C. Lin, "Chemical HF lasers from NF$_3$–H$_2$ and NF$_3$–C$_2$H$_6$ systems," J. Chem. Phys. **75**, 284–286 (1971).

[11]A. M. Razhev, D. S. Churkin, E. S. Kargapol'tsev, and S. V. Demchuk, "Pulsed inductive HF laser," Quantum Electron. **46**, 210–212 (2016).

[12]N. Posseme, V. Ah-Leung, O. Pollet, C. Arvet, and M. Garcia-Barros, "Thin layer etching of silicon nitride: A comprehensive study of selective removal using NH$_3$/NF$_3$ remote plasma," J. Vac. Sci. Technol., A **34**, 061301 (2016).

[13]K.-C. Yang, S.-W. Park, and G.-Y. Yeom, "Low global warming potential alternative gases for plasma chamber cleaning," Sci. Adv. Mater. **8**, 2253–2259 (2016).

[14]C. Szmytkowski, A. Domaracka, P. Możejko, E. Ptasińska-Denga, Ł. Kłosowski, M. Piotrowicz, and G. Kasperski, "Electron collisions with nitrogen trifluoride NF$_3$ molecules," Phys. Rev. A **70**, 032707 (2004).

[15]L. Boesten, Y. Tachibana, Y. Nakano, T. Shinohara, H. Tanaka, and M. Dillon, "Vibrationally inelastic and elastic cross sections for e^--NF$_3$ collisions," J. Phys. B: At., Mol. Opt. Phys. **29**, 5475–5492 (1996).

[16]V. Tarnovsky, A. Levin, K. Becker, R. Basner, and M. Schmidt, "Electron impact ionization of the NF$_3$ molecule," Int. J. Mass Spectrom. **133**, 175–185 (1994).

[17]P. D. Haaland, C. Q. Jiao, and A. Garscadden, "Ionization of NF$_3$ by electron impact," Chem. Phys. Lett. **340**, 479 (2001).

[18]M. Rahman, S. Gangopadhyay, C. Limbachiya, K. Joshipura, and E. Krishnakumar, "Electron ionization of NF$_3$," Int. J. Mass Spectrom. **319**, 48–54 (2012).

[19]P. W. Harland and J. L. Franklin, "Partitioning of excess energy in dissociative resonance capture processes," J. Chem. Phys. **61**, 1621–1636 (1974).

[20]D. Nandi, S. A. Rangwala, S. V. K. Kumar, and E. Krishnakumar, "Absolute cross sections for dissociative electron attachment to NF$_3$," Int. J. Mass Spectrom. **205**, 111–117 (2001).

[21]P. Chantry, "Dissociative attachment cross-section measurements in F$_2$ and NF$_3$," Bull. Am. Phys. Soc. **24**, 134 (1979).

[22]T. N. Rescigno, "Low-energy electron collision processes in NF$_3$," Phys. Rev. A **52**, 329–333 (1995).

[23]E. Joucoski and M. H. F. Bettega, "Elastic scattering of low-energy electrons by NF$_3$," J. Phys. B: At., Mol. Opt. Phys. **35**, 783–793 (2002).

[24]B. Goswami, R. Naghma, and B. Antony, "Cross sections for electron collisions with NF$_3$," Phys. Rev. A **88**, 032707 (2013).

[25]J. R. Hamilton, J. Tennyson, S. Huang, and M. J. Kushner, "Calculated cross sections for electron collisions with NF$_3$, NF$_2$ and NF," Plasma Sources Sci. Technol. **26**, 065010 (2017).

[26]V. Lisovskiy, V. Yegorenkov, P. Ogloblina, J.-P. Booth, S. Martins, K. Landry, D. Douai, and V. Cassagne, "Electron transport parameters in NF$_3$," J. Phys. D: Appl. Phys. **47**, 115203 (2014).

[27]R. D. Johnson, "NIST computational chemistry comparison and benchmark database, NIST standard reference database number 101," Release 17b, III (2015).

[28]S. E. Novick, W. Chen, M. R. Munrow, and K. J. Grant, "Hyperfine structure in the microwave spectrum of NF$_3$," J. Mol. Spectrosc. **179**, 219–222 (1996).

[29]*CRC Handbook of Chemistry and Physics*, edited by F. Macdonald and D. Lide (CRC Press, Boca Raton, 2003-2004).

[30]D. H. Shi, J. F. Sun, Z. L. Zhu, and Y. F. Liu, "Total cross sections of electron scattering by molecules NF$_3$, PF$_3$, N(CH$_3$)$_3$, P(CH$_3$)$_3$, NH(CH$_3$)$_2$, PH(CH$_3$)$_2$, NH$_2$CH$_3$ and PH$_2$CH$_3$ at 30-5000 eV," Eur. Phys. J. D **57**, 179–186 (2010).

[31]G. Karwasz, T. Wróblewski, R. Brusa, and E. Illenberger, "Electron scattering on triatomic molecules: The need for data," Jpn. J. Appl. Phys., Part 1 **45**, 8192 (2006).

[32]M. H. F. Bettega, C. Winstead, and V. McKoy, "Low-energy electron scattering by N$_2$O," Phys. Rev. A **74**, 022711 (2006).

[33]M.-Y. Song, J.-S. Yoon, H. Cho, Y. Itikawa, G. P. Karwasz, V. Kokoouline, Y. Nakamura, and J. Tennyson, "Cross sections for electron collisions with methane," J. Phys. Chem. Ref. Data **44**, 023101 (2015).

[34]A. Zecca, G. Karwasz, R. Brusa, and R. Grisenti, "Absolute total cross section measurements for intermediate-energy electron scattering. IV. Kr and Xe," J. Phys. B: At., Mol. Opt. Phys. **24**, 2737 (1999).

[35]A. Zecca, G. P. Karwasz, and R. S. Brusa, "Electron scattering by Ne, Ar and Kr at intermediate and high energies, 0.5-10 keV," J. Phys. B: At., Mol. Opt. Phys. **33**, 843 (2000).

[36]J. Tennyson, D. B. Brown, J. J. Munro, I. Rozum, H. N. Varambhia, and N. Vinci, "Quantemol-N: An expert system for performing electron molecule collision calculations using the R-matrix method," J. Phys. Conf. Series **86**, 012001 (2007).

[37]J. M. Carr, P. G. Galiatsatos, J. D. Gorfinkiel, A. G. Harvey, M. A. Lysaght, D. Madden, Z. Masin, M. Plummer, and J. Tennyson, "UKRmol: A low-energy electron- and positron-molecule scattering suite," Eur. Phys. J. D **66**, 58 (2012).

[38]D. T. Stibbe and J. Tennyson, "Near-threshold electron impact dissociation of H$_2$," New J. Phys. **1**, 2 (1998).

[39]V. I. Vedeneyev, L. V. Gurvich, V. N. Kondrat'ev, V. A. Medvedev, and E. L. Frankevich, "Chemical Bond Energies, Ionization Potentials and Electron Affinities" (Edward Arnold, Ltd., London, 1966), translation of 1962 Russian edition.

[40]A. Kennedy and C. B. Colburn, "Strength of the N–F bonds in NF$_3$ and of N–F and N–N bonds in N$_2$F$_4$," J. Chem. Phys. **35**, 1892–1893 (1961).

[41]W. J. Brigg, J. Tennyson, and M. Plummer, "R-matrix calculations of low-energy electron collisions with methane," J. Phys. B: At., Mol. Opt. Phys. **47**, 185203 (2014).

[42]S.-I. Chu and A. Dalgarno, "Rotational excitation of CH$^+$ by electron impact," Phys. Rev. A **10**, 788–792 (1974).

[43]K. L. Baluja, N. J. Mason, L. A. Morgan, and J. Tennyson, "Electron scattering from ClO using the R-matrix method," J. Phys. B: At., Mol. Opt. Phys. **33**, L677–L684 (2000).

[44]D. P. Seccombe, R. P. Tuckett, H.-W. Jochims, and H. Baumgärtel, "The observation of fluorescence from excited states of NF$_2$ and NF following the photodissociation of NF$_3$ in the 11–30 eV range," Chem. Phys. Lett. **339**, 405–412 (2001).

[45]Y.-K. Kim and M. E. Rudd, "Binary-encounter-dipole model for electron-impact ionization," Phys. Rev. A **50**, 3954–3967 (1994).

[46]M. T. Elford, in *Photon and Electron Interactions with Atoms, Molecules, and Ions, Landolt-Börnstein: Numerical Data and Functional Relation-ships in Science and Technology/Elementary Particles, Nuclei and Atoms*, edited by W. Martinenssen (Springer, New York, 2003), Vol. 17.

[47]V. Tarnovsky, A. Levin, and K. Becker, "Absolute cross sections for the electron impact ionization of the NF$_2$ and NF free radicals," J. Chem. Phys. **100**, 5626–5630 (1994).

[48]R. C. Wetzel, F. A. Baiocchi, T. R. Hayes, and R. S. Freund, "Absolute cross sections for electron-impact ionization of the rare-gas atoms by the fast-neutral-beam method," Phys. Rev. A **35**, 559–577 (1987).

[49]E. Krishnakumar and S. K. Srivastava, "Ionisation cross sections of rare-gas atoms by electron impact," J. Phys. B: At., Mol. Opt. Phys. **21**, 1055–1082 (1988).

[50]M. R. Bruce and R. A. Bonham, "On the partial ionization cross-sections for CF$_4$ by use of the pulsed-electron-beam time-of-flight method," Int. J. Mass Spectrom. **123**, 97–100 (1993).

[51]W. M. Huo, V. Tarnovsky, and K. H. Becker, "Total electron-impact ionization cross-sections of CF$_x$ and NF$_x$ (x = 1–3)," Chem. Phys. Lett. **358**, 328–336 (2002).

[52]G. P. Karwasz, P. Możejko, and M.-Y. Song, "Electron-impact ionization of fluoromethanes—Review of experiments and binary-encounter models," Int. J. Mass Spectrom. **365**, 232–237 (2014).

[53]R. M. Reese and V. H. Dibeler, "Ionization and dissociation of nitrogen trifluoride by electron impact," J. Chem. Phys. **24**, 1175–1177 (1956).

[54]K. Nygaard, H. Brooks, and S. Hunter, "Negative ion production rates in rare gas-halide lasers," IEEE J. Quantum Electron. **15**, 1216–1223 (1979).

[55]V. K. Lakdawala and J. L. Moruzzi, "Measurements of attachment co-efficients in NF$_3$ -nitrogen and NF$_3$ -rare gas mixtures using swarm tech-niques," J. Phys. D: Appl. Phys. **13**, 377–386 (1980).

[56]N. Ruckhaberle, L. Lehmann, S. Matejcik, E. Illenberger, Y. Bouteiller, V. Periquet, L. Museur, C. Desfrançois, and J.-P. Schermann, "Free electron attachment and Rydberg electron transfer to NF$_3$ molecules and clusters," J. Phys. Chem. A **101**, 9942–9947 (1997).

[57]M.-Y. Song, J.-S. Yoon, H. Cho, Y. Itikawa, G. P. Karwasz, V. Kokoouline, Y. Nakamura, and J. Tennyson, "Cross sections for electron collisions with acetylene," J. Phys. Chem. Ref. Data **46**, 013106 (2017).